DOI:
10.1002/mrm.24463

Document Version
Publisher's PDF, also known as Version of record

PRECLINICAL AND CLINICAL IMAGING – Full Papers

Magnetic Resonance in Medicine 70:504–516 (2013)

Motion Corrected Compressed Sensing for Free-Breathing Dynamic Cardiac MRI

Muhammad Usman,[1]* David Atkinson,[2] Freddy Odille,[3] Christoph Kolbitsch,[1] Ghislain Vaillant,[1] Tobias Schaeffter,[1] Philip G. Batchelor,[1] and Claudia Prieto[1,4]

Compressed sensing (CS) has been demonstrated to accelerate MRI acquisitions by reconstructing sparse images of good quality from highly undersampled data. Motion during MR scans can cause inconsistencies in k-space data, resulting in strong motion artifacts in the reconstructed images. For CS to be useful in these applications, motion correction techniques need to be combined with the undersampled reconstruction. Recently, joint motion correction and CS approaches have been proposed to partially correct for effects of motion. However, the main limitation of these approaches is that they can only correct for affine deformations. In this work, we propose a novel motion corrected CS framework for free-breathing dynamic cardiac MRI that incorporates a general motion correction formulation directly into the CS reconstruction. This framework can correct for arbitrary affine or nonrigid motion in the CS reconstructed cardiac images, while simultaneously benefiting from highly accelerated MR acquisition. The application of this approach is demonstrated both in simulations and in vivo data for 2D respiratory self-gated free-breathing cardiac CINE MRI, using a golden angle radial acquisition. Results show that this approach allows for the reconstruction of respiratory motion corrected cardiac CINE images with similar quality to breath-held acquisitions. **Magn Reson Med 70:504–516, 2013.** © **2012 Wiley Periodicals, Inc.**

Key words: compressed sensing; undersampling; motion correction; nonrigid motion; dynamic cardiac MRI

INTRODUCTION

Compressed sensing (CS) has been recently proposed and applied to speed up the acquisition of MR images (1–3). Its use has been successfully demonstrated in several MR applications where the images are sparse in themselves or in some transform representation. Applications include brain (3), cardiac (4), coronary (5), and pediatric MR imaging (6), among others. In all these applications, motion artifacts such as blurring and ghosting can be introduced in the MR image reconstruction due to unwanted or involuntary movement during acquisition. In free-breathing cardiac gated MR acquisitions, different k-space profiles belonging to a specific cardiac phase are acquired at distinctive breathing positions or "motion states." The combination of profiles from the same cardiac phase but different respiratory motion states can result in inconsistencies in k-space, leading to motion artifacts in the reconstructed images. In addition, this unwanted motion can also reduce the sparsity level of MR images in the sparse representation, thus reducing the acceleration factor achievable with CS reconstruction (7). Hence, to benefit from the high acceleration available from CS methods in these applications, additional flexibility is required to combine motion correction with the CS reconstruction.

Some approaches to combine CS reconstruction with motion correction techniques have been recently proposed (7,8). Jung et al. proposed a CS technique "k-t FOCal Underdetermined System Solver (FOCUSS)" (9–11) that incorporated a motion estimation procedure to predict different cardiac phases from a fully sampled reference cardiac frame. The knowledge of motion between cardiac phases was mainly used to enhance the sparsity in the sparse representation for better CS reconstruction. This framework was demonstrated for breath-hold CINE, where all data were acquired in one respiratory motion state (i.e., end expiration) and hence, there was no issue of motion corruption due to inconsistencies among the acquired k-space data. For free-breathing 2D cardiac MRI where data are acquired in different respiratory motion states, Otazo et al. proposed a combination of CS and parallel imaging with 1D translational respiratory motion correction (7). For 3D static coronary imaging, Doneva et al. (8) proposed a method that performed CS reconstruction from data acquired in each motion state and afterward averaged the CS reconstructed images following image based affine registration. However, in general, the motion can be arbitrary affine or nonrigid. Hence, a CS-based motion correction framework is needed that can correct for arbitrary nonrigid motion in the CS reconstruction using data acquired at multiple motion states.

In 2005, Batchelor et al. (12) introduced a generalized motion correction framework that can correct for general (affine or nonrigid) motion in the image reconstruction. This framework modeled the transformation from the motion free image to the acquired motion corrupted k-space samples at different motion states via a matrix-vector equation. Provided, the motion (affine or nonrigid) itself is known, standard numerical matrix inversion

[1]King's College London, Division of Imaging Sciences and Biomedical Engineering, British Heart Foundation (BHF) Centre of Excellence, Medical Engineering Centre of Research Excellence, London, UK.

[2]University College London, Centre for Medical Imaging, London, UK.

[3]IADI, Inserm U974, Nancy University Hospital, Nancy, France.

[4]Pontificia Universidad Católica de Chile, Escuela de Ingeniería, Santiago, Chile.

Grant sponsor: EPSRC; Grant number: EP/H046410/1; Grant sponsor: FONDECYT; Grant number: 11110053.

*Correspondence to: Muhammad Usman, Ph.D., Division of Imaging Sciences and Biomedical Engineering, The Rayne Institute, 4th Floor, Lambeth Wing, St. Thomas' Hospital, London SE1 7EH, UK. E-mail: muhammad.usman@kcl.ac.uk

Received 11 June 2012; revised 10 July 2012; accepted 24 July 2012.

DOI 10.1002/mrm.24463

Published online 16 August 2012 in Wiley Online Library (wileyonlinelibrary.com).

algorithms can be used to reconstruct a motion corrected image. Using information from multiple coils in parallel MRI, the application of this framework has been recently demonstrated in brain imaging (12), coronary MRI (13), cardiac CINE (14–16), and liver MRI (17) to correct for nonrigid motion.

In this work, we propose a novel motion corrected-compressed sensing (MC-CS) framework for free-breathing dynamic cardiac MRI, which incorporates a generalized motion correction formulation directly into the CS reconstruction. This framework can correct for general (affine or nonrigid) motion in the cardiac images reconstructed from CS undersampled respiratory motion-corrupted k-space data. To separate parallel imaging effects from CS, the acquired data from a single element of a multicoil array are considered in this work. The number of acquired k-space samples in each motion state is below the Nyquist rate. The framework was tested using a respiratory self-gated golden angle radial acquisition (18). This acquisition allows for the reconstruction of images with arbitrary temporal resolution, a property that can be exploited for self-gating and motion estimation. The golden radial acquisition also satisfies the pseudorandom sampling required by CS reconstruction (19). The usefulness of MC-CS framework is demonstrated both in simulations and in vivo free-breathing 2D cardiac CINE MRI.

THEORY

Batchelor et al. (12) proposed an exact formulation for the effect of any motion during acquisition of k-space that is described as follows: let $\mathbf{s}$ be the motion-free image to be reconstructed, $\mathbf{y}$ the motion corrupted k-space data and assume D possible motion states ($d = 1, 2, 3, \ldots, D$) of the underlying object. The motion corrupted k-space data $\mathbf{y}$ consists of the sum of the k-space samples acquired over all the motion states (12):

$$\mathbf{y} = \sum\nolimits_d \mathbf{A}_d \mathbf{F}^{\mathbf{s}} \mathbf{U}_d \mathbf{s} \qquad [1]$$

where, $\mathbf{U}_d$ is a motion matrix that warps the pixels in image $\mathbf{s}$ (reference) to the position at the dth motion state, $\mathbf{F}^{\mathbf{s}}$ is the 2D Fourier encoding matrix that transforms the warped image to the k-space, and $\mathbf{A}_d$ is the undersampling operator that selects the k-space samples acquired at motion state d. For non-Cartesian acquisitions, $\mathbf{A}_d$ also includes the gridding operation.

Considering a free-breathing CINE acquisition with N retrospectively assigned cardiac phases and D respiratory positions, similar to Eq. 1, the motion corrupted undersampled k-space data ($\mathbf{y}_n$) for each cardiac phase $n = 1, 2, \ldots, N$ correspond to:

$$\mathbf{y}_n = \sum\nolimits_d \mathbf{A}_{d,n} \mathbf{F}^{\mathbf{s}} \mathbf{U}_{d,n} \mathbf{s}_n = \mathbf{E}_n \mathbf{s}_n \qquad [2]$$

where $\mathbf{s}_n$ is the motion-corrected image for cardiac phase "n," $\mathbf{U}_{d,n}$ is the matrix describing the general (affine or nonrigid) motion of cardiac phase n ($n = 1, 2, \ldots, N$) from a reference respiratory position (usually at end expiration) to the dth respiratory position ($d = 1, 2, \ldots, D$), $\mathbf{F}^{\mathbf{s}}$ is the 2D spatial Fourier encoding matrix, $\mathbf{A}_{d,n}$ is the pseudorandom sampling pattern at the dth respiratory position for the cardiac phase n and includes the gridding operation for non-Cartesian acquisitions, and $\mathbf{E}_n$ is the encoding operator given by $\mathbf{E}_n = \sum_d \mathbf{A}_{d,n} \mathbf{F}^{\mathbf{s}} \mathbf{U}_{d,n}$. For a specific cardiac phase n and a particular respiratory position d, the sampling given by $\mathbf{A}_{d,n}$ does not satisfy the Nyquist criterion. The corresponding undersampling factor varies for each respiratory position d according to the breathing cycle, being lower for the most probable breathing states (i.e., end-expiration) and higher for other motion states.

The MR dynamic cardiac images are sparse in the 3D spatio-temporal domain x–y–f space (x,y: spatial position, f: temporal frequency; Refs. 4 and 20) due to the quasiperiodic motion of the heart. Exploiting sparsity in the x–y–f space, the proposed MC-CS formulation to recover the respiratory motion-corrected cardiac phases is given as:

$$\min_{\mathbf{s}} ||\mathbf{F}^{\mathbf{t}} \mathbf{s}||_1 \quad \mathbf{s.t.} \; ||\mathbf{y} - \mathbf{E}\mathbf{s}||_2 \leq \sigma \qquad [3]$$

where $\mathbf{y} = \begin{bmatrix} \mathbf{y}_1 \\ \mathbf{y}_2 \\ \vdots \\ \mathbf{y}_N \end{bmatrix}$, $\mathbf{E} = \begin{bmatrix} \mathbf{E}_1 & & & \\ & \mathbf{E}_2 & & \\ & & \ddots & \\ & & & \mathbf{E}_N \end{bmatrix}$, and $\mathbf{s} = \begin{bmatrix} \mathbf{s}_1 \\ \mathbf{s}_2 \\ \vdots \\ \mathbf{s}_N \end{bmatrix}$ include all N cardiac phases, $\mathbf{F}^{\mathbf{t}}$ is the temporal Fourier operator that transforms the signal $\mathbf{s}$ from the x–y–t space to the sparse x–y–f space by applying the Fourier transform along the temporal dimension, $||.||_1$ denotes the l_1 norm given as the sum of absolute values of all elements in the sparse representation, $||.||_2$ denotes the l_2 norm, σ is a parameter that controls the fidelity of the reconstruction to the measured data and is usually set below the expected noise level. The difference between this formulation and the standard CS reconstruction is that the encoding operator $\mathbf{E}$ includes the motion information $\mathbf{U}_{d,n}$ and uses data from all the motion states.

Using the motion information embedded in $\mathbf{U}_{d,n}$, the MC-CS formulation given in Eq. 3 finds the sparsest solution in the x–y–f space. Here, for simplicity, we have assumed independence of motion between cardiac phases in any R–R interval as has been previously assumed in the literature (14,15,21,22). The above formulation is independent of the acquisition trajectory, provided the motion information $\mathbf{U}_{d,n}$ is available and a pseudorandom undersampled acquisition is performed.

METHODS

We propose a new framework for respiratory motion corrected reconstruction in 2D dynamic cardiac CINE MRI. The basic strategy is to acquire free-breathing cardiac data for a number of cardiac cycles and reconstruct a cardiac CINE free of respiratory motion. To apply MC-CS formulation (as defined in Eq. 3) for general (affine or nonrigid) motion correction, the k-space profiles in the acquired free-breathing cardiac MR data have to be

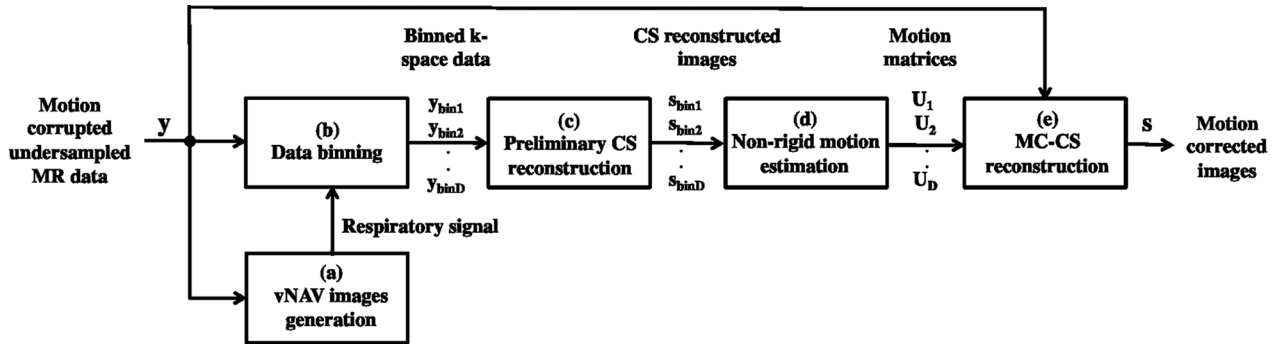

FIG. 1. Block diagram of the proposed MC-CS framework for dynamic cardiac MRI using golden radial acquisition. **a:** A respiratory signal is estimated from virtual navigator (vNAV) images reconstructed from the acquired k-space data **y**. **b:** The respiratory signal allows binning of the acquired data **y** into D motion states/bins. **c:** From the acquired data binned into D different motion states ($\mathbf{y}_{bin1}$, $\mathbf{y}_{bin2}$, ..., $\mathbf{y}_{binD}$), a preliminary CS reconstruction (without motion correction) is performed independently for each bin. **d:** The CS reconstructed images in a reference bin are registered to the images in other bins to generate the motion matrices $\mathbf{U}_1$, $\mathbf{U}_2$, ..., $\mathbf{U}_D$. **e:** Employing the acquired data **y** and the motion matrices $\mathbf{U}_d$'s ($d = 1, 2, \ldots, D$), the final MC-CS reconstruction is performed yielding motion corrected image **s**.

associated/binned into different motion states $d = 1, 2, \ldots, D$ such that respiratory motion within each motion state can be assumed small enough to not cause motion-artifacts in images reconstructed from the data. Thus, binning of data resolves inconsistencies among k-space data in each motion state. The motion between different motion states can be estimated by first reconstructing the images at each motion state and then registering these images to get the motion information **U**.

An image based respiratory signal (obtained, e.g., from external navigator on diaphragm or from acquired data itself as self-gated signal) acts as a surrogate of respiratory motion in the head–feet (H–F) direction and hence can be used for data binning (22). Within each motion state, separate CS reconstructions are performed. The most common respiratory motion state is chosen as the reference, and all the CS reconstructions are nonrigidly registered to this reference. The registrations provide an estimate of motion and the MC-CS formulation in Eq. 3 can be used to reconstruct images free of respiratory motion. The golden angle radial based acquisition (18) is used, because it ensures the k-space sample locations for different k-space profiles for a particular cardiac phase n and a respiratory position "d" are mutually exclusive (except for the center point in k-space) in subsequent R–R intervals, thus allowing flexibility in the reconstruction. Moreover, the reconstruction flexibility of this trajectory allows estimation of respiratory surrogate from the same acquired data.

To summarize, the proposed MC-CS framework for free-breathing dynamic cardiac MRI can be divided into five different steps: (a) a respiratory signal for data binning is estimated by rigid registration of low resolution virtual 2D navigator (vNAV) images reconstructed from the acquired data; (b) the acquired k-space profiles are binned into different motion states (or bins) based on vNAV position and a selected reference bin; (c) preliminary CS reconstructions without motion correction are performed from binned k-space data for each motion state; (d) preliminary CS reconstructed CINE images for the reference bin are registered to preliminary CS reconstructed CINE images in each bin via nonrigid registration that yields the required respiratory motion fields; (e) MC-CS reconstruction (Eq. 3) is performed using motion information and data available from all the bins to obtain the final motion corrected CINE images. These different steps are shown as a block diagram in Figure 1 and further described later.

vNAV Images Generation

To generate a navigator signal for data binning, low temporal resolution vNAV images are generated by combining golden angle radial profiles for each R–R interval over the whole respiratory cycle. Respiratory translational displacement is estimated doing a rigid registration of these vNAV images (22). Registration is performed on a region of interest (ROI) containing the heart using the respiratory position of the first vNAV image as reference (Fig. 2). An example respiratory navigator signal obtained from free-breathing data containing 35 cardiac cycles is shown in Figure 3. Each value in the signal represents the average position of the heart during the respective heartbeat.

Data Binning

The acquired radial profiles from all heartbeats are binned into a number of respiratory motion states/bins according to the breathing position at which these were acquired, given by the vNAV images. The number of bins should be as large as possible to minimize intrabin motion, and at the same time the width of each bin should be large enough to ensure that it has sufficient data for image reconstruction.

There are two strategies available in the literature for data binning: (a) uniform data binning and (b) adaptive data binning. The standard uniform binning procedure (23) uses bins of equal width. As the breathing patterns can be irregular, the uniform data binning may lead to some bins having a reduced amount of data and hence reconstructions with undersampling artifacts in those bins. These reconstructed images with artifacts lead to registration errors in the motion estimation step. To

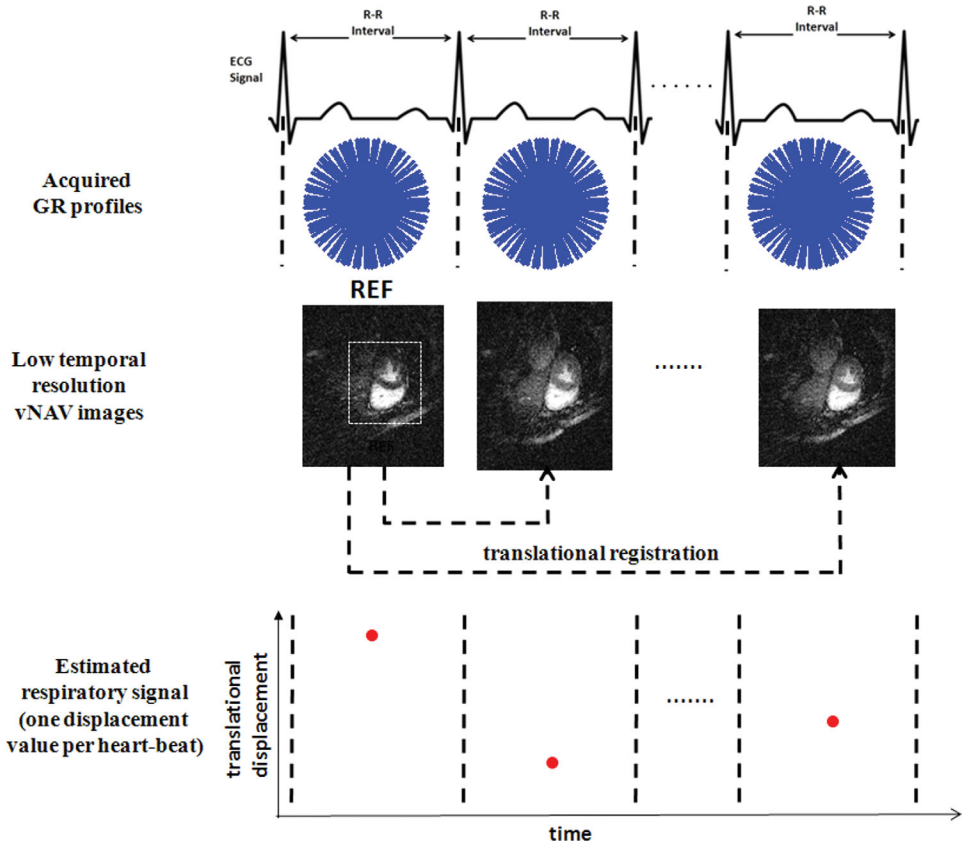

FIG. 2. An illustration of respiratory signal estimation with the proposed method for dynamic cardiac MRI. Low resolution vNAV images were reconstructed from golden angle radial profiles acquired in every heart beat. Rigid translational registration is performed on a ROI containing the heart using the first vNAV image in the sequence as the reference. This generates a respiratory signal that contains one average displacement value per heart beat. [Color figure can be viewed in the online issue, which is available at wileyonlinelibrary.com.]

avoid this issue, another strategy is to use adaptive binning of acquired data with overlapping bins. This has been used in a recent work (24) with golden angle radial phase encoding trajectory, where the width of each bin was arbitrarily adjusted to include more profiles improving the sampling density of each bin. Due to the flexibility of the golden radial trajectory, the data binning can be used in an overlapped fashion, because data from adjacent bins are complimentary and hence can be combined. The advantage of using overlapping binning is that a higher number of bins can be reconstructed to describe the respiratory motion.

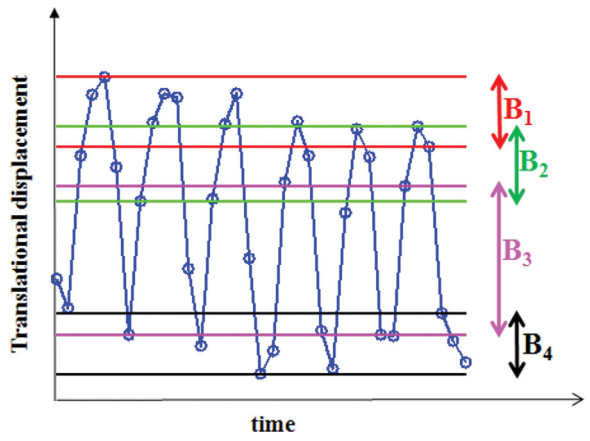

FIG. 3. Data binning step of proposed method: an example respiratory signal estimated from free-breathing data acquired over 35 heart beats is shown. The data are grouped into four overlapped bins (B_1–B_4), each bin comprising data from 11 heart beats, with data acquired over three heart beats shared between the adjacent bins. This results in bins of different sizes, the bin-width being dependent on the spread of the navigator displacement values in that bin. [Color figure can be viewed in the online issue, which is available at wileyonlinelibrary.com.]

In our work, we use a similar adaptive overlapping binning strategy based on the spread of the displacement values in the respiratory signal. To satisfy the requirements of data binning, the total number of bins P is defined such that data in each bin correspond to equal number of heart beats and the amount of data in each bin is sufficient to ensure good CS reconstructed images (4–6 times undersampling compared to Nyquist rate). This can be done by sorting the displacement values in the respiratory signal and grouping the profiles acquired in heart beats corresponding to the sorted displacement values into P bins. The grouping can be done in overlapping fashion to increase the total number of bins. Increasing the number of heart beats will increase the number of bins, as finer resolution bins can be formed that satisfy the CS sampling requirements. The reference bin is selected to be the one with smallest bin width, as it will have least amount of intra bin motion.

An example data binning is shown in Figure 3. The data were grouped into four overlapping bins (B_1–B_4),

each bin comprising data from 11 heart beats, with shared data of three heart beats from the adjacent bins. This resulted in bins of different sizes, with the bin-width depending on the breathing pattern.

Preliminary CS Reconstruction

Data within each motion state/bin are retrospectively assigned to N cardiac phases based on an external electrocardiogram (ECG) signal. For each motion state, the data are in k_x–k_y–t space, where time index "t" in k_x–k_y–t refers to the cardiac phase index n rather than real time. A preliminary CS reconstruction (k–t Sparse; Ref. 4), without motion correction is performed for each bin independently, with the 3D x–y–f space as the sparse representation. This step reconstructs N cardiac phases for each respiratory motion state. To transform data from k_x–k_y–t to the x–y–f space, first the k-space data for each time index t are transformed (gridded since a non-Cartesian trajectory is used) to the image space. Then, a Fourier transform is taken along the temporal direction to get the x–y–f space representation.

Motion Estimation

Each CS reconstructed cardiac phase n at the reference respiratory position is registered to the corresponding cardiac phase n at other respiratory positions ($d = 1, 2, \ldots, D$) using an efficient intensity-based nonrigid registration algorithm (25). This algorithm achieves nonrigid motion estimations by combining multiple local affine registrations. Pixel-wise motion fields for every cardiac phase within each bin are obtained from the registration process. These motion fields are used to construct the motion matrices $\mathbf{U}_{d,n}$'s. Each row of the matrix $\mathbf{U}_{d,n}$ contains mostly zeros except for those columns corresponding to the pixels in the reference image that would contribute to a given pixel in the warped image at the dth motion state. The number of nonzero entries in each row is determined by the size of the interpolation kernel. In case of bilinear interpolation used in this work, there are only four nonzero entries in each row of $\mathbf{U}_{d,n}$.

MC-CS Reconstruction

Using estimated $\mathbf{U}_{d,n}$'s and acquired data $\mathbf{y}$ from all the motion states, the final MC-CS reconstruction is performed using Eq. 3, to yield the motion-corrected retrospectively reordered cardiac image sequence.

The preliminary CS reconstruction, motion estimation, and MC-CS reconstruction steps are illustrated in Figure 4.

EXPERIMENTS

The proposed method was tested on simulated and in vivo free breathing retrospectively cardiac gated 2D cardiac CINE MR data. To demonstrate that MC-CS framework can correct for arbitrary nonrigid motion in the reconstruction, cardiac data acquired during breath-hold were motion-corrupted by different nonrigid deformations in the simulations. In both simulations and in vivo experiments, the performance of the MC-CS framework was compared against CS reconstructions from free-breathing data without motion correction (CS + no MC) and the CS reconstruction from breath-held acquisition (BH-CS). In all cases, the x–y–f space was used as the sparse representation. The acceleration factors mentioned or shown in the text and figures indicate the acceleration factors relative to the radial Nyquist sampling rate ($\pi/2$ times the number of frequency encoding points).

Reconstruction

All reconstructions were implemented in MATLAB (R2010, The MathWorks, Inc., Natick, MA) on a work station with a six core processor, Intel Xeon X5670, 2.93 GHz, and 24 GB memory using a nonlinear conjugate gradient reconstruction algorithm with backtracking line-search (3). The nonlinear conjugate gradient algorithm solves the following unconstrained Hermitian-symmetric form of problem in Eq. 3 expressed as:

$$\min_{\mathbf{s}} \lambda ||\mathbf{F}^{\mathbf{t}}\mathbf{s}||_1 + ||\mathbf{E}^{\mathrm{H}}\mathbf{y} - \mathbf{E}^{\mathrm{H}}\mathbf{E}\mathbf{s}||_2^2 \quad [4]$$

where λ is a regularization parameter that selects the trade-off between the sparsity of the underlying signal $\mathbf{s}$ in x–y–f space and data consistency, and $\mathbf{E}$ is the encoding operator. The Hermitian-symmetric form:

$$\mathbf{E}^{\mathrm{H}}\mathbf{y} = \mathbf{E}^{\mathrm{H}}\mathbf{E}\mathbf{s} \quad [5]$$

is considered for data consistency in Eq. 4, with $\mathbf{E}^{\mathrm{H}}\mathbf{y} = \begin{bmatrix} \mathbf{E}_1^{\mathrm{H}}\mathbf{y}_1 \\ \mathbf{E}_2^{\mathrm{H}}\mathbf{y}_2 \\ \vdots \\ \mathbf{E}_N^{\mathrm{H}}\mathbf{y}_N \end{bmatrix}$ and $\mathbf{E}^{\mathrm{H}}\mathbf{E} = \begin{bmatrix} \mathbf{E}_1^{\mathrm{H}}\mathbf{E}_1 & & & \\ & \mathbf{E}_2^{\mathrm{H}}\mathbf{E}_2 & & \\ & & \ddots & \\ & & & \mathbf{E}_N^{\mathrm{H}}\mathbf{E}_N \end{bmatrix}$, where $\mathbf{E}_n^H\mathbf{y}_n = \sum_d \mathbf{U}_{d,n}^H(\mathbf{F}^{\mathbf{s}})^H\mathbf{A}_{d,n}^H\mathbf{y}_n$ and $\mathbf{E}_n^H\mathbf{E}_n = \sum_d \mathbf{U}_{d,n}^H(\mathbf{F}^{\mathbf{s}})^H \mathbf{A}_{d,n}^H\mathbf{A}_{d,n}(\mathbf{F}^{\mathbf{s}})\mathbf{U}_{d,n}$ for $n = 1, 2, \ldots, N$. Here $(\mathbf{F}^{\mathbf{s}})^{\mathrm{H}}$ is the 2D inverse Fourier encoding matrix that transforms data from k-space to the image domain and $\mathbf{U}_{d,n}^{\mathrm{H}}$ is the Hermitian of $\mathbf{U}_{d,n}^{\mathrm{H}}$, which may be approximated as inverse motion transformation matrix.

In our simulations, the optimal value range for λ (0.04–0.07) was determined by comparing reconstructions with different λ's to the fully sampled ground truth. In all simulations and in vivo experiments, λ was chosen from this range and set to the same value for preliminary CS reconstructions and the final MC-CS reconstruction.

The gridding and degridding steps in the encoding operators $\mathbf{E}$ and $\mathbf{E}^{\mathrm{H}}$ were implemented using Kaiser-Bessel gridding kernel as proposed in Ref. 26, and the density compensation functions were numerically estimated using Voronoi diagrams (27).

Simulations

In the simulations, the performance of MC-CS reconstruction framework as a function of the acceleration factor was investigated. In addition, the effect of acceleration on the accuracy of nonrigid registration in the motion estimation step of the proposed method was also analyzed.

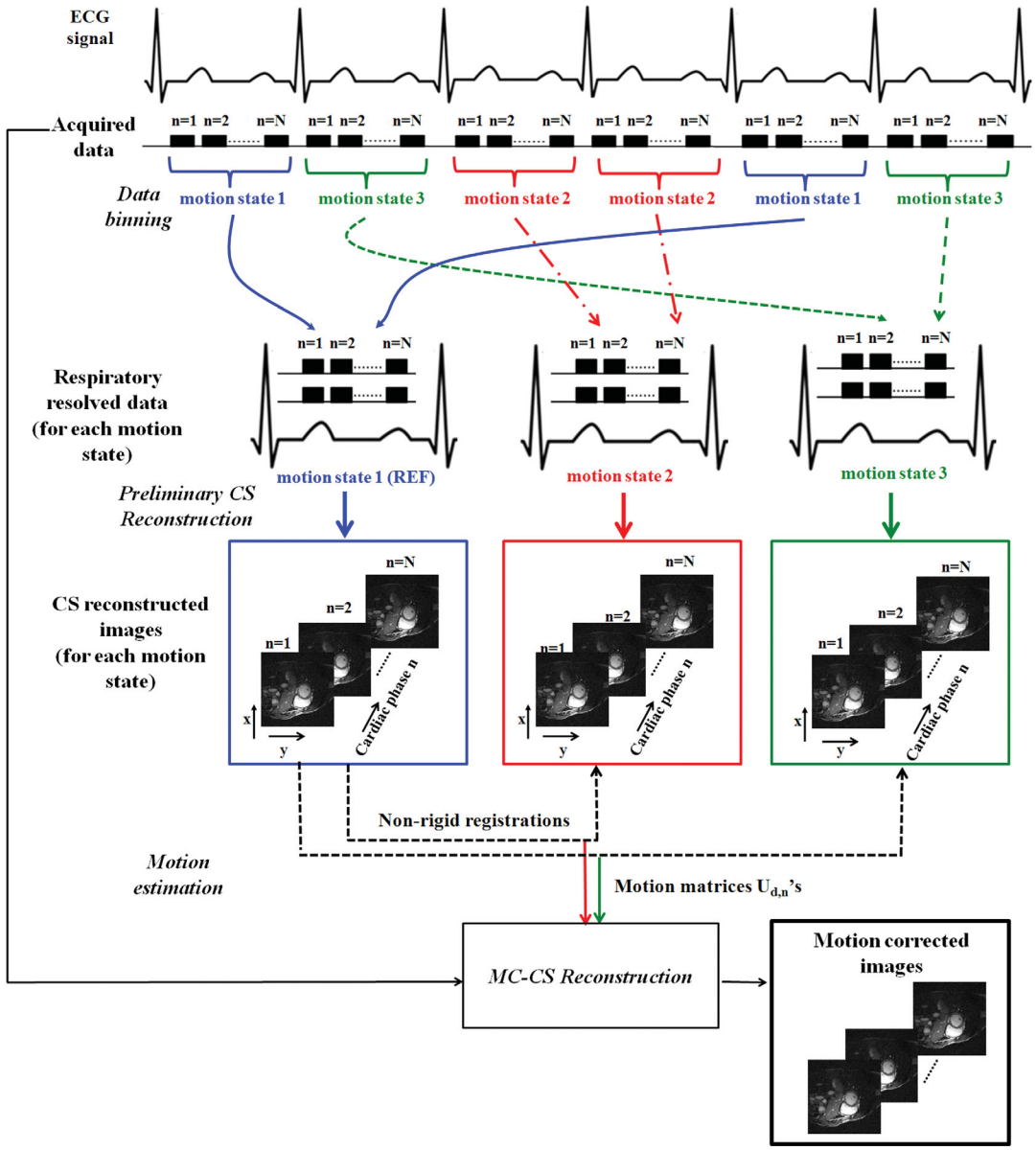

FIG. 4. An illustration of preliminary CS reconstruction, motion estimation, and MC-CS reconstruction steps of the proposed framework. For simplicity, only three motion states and six heart beats are shown here. The data binning step assigns data acquired in each heart beat to one of the three motion states. Hence, after the data binning step, the respiratory resolved data for each motion state are obtained. Here, the motion state 1 is assumed to be the reference (REF). Preliminary CS reconstruction is done for each respiratory motion state, yielding N reconstructed cardiac phases for each motion state. Each cardiac phase n in reference motion state 1 is registered to the corresponding cardiac phase at respiratory motion states 2 and 3 to yield motion fields. Using these motion fields and the acquired data, MC-CS reconstruction recovers the respiratory motion-free CINE images. [Color figure can be viewed in the online issue, which is available at wileyonlinelibrary.com.]

Golden angle radial motion corrupted data were simulated from cardiac gated breath-held CINE data acquired at end-expiration on a Philips 1.5T Achieva scanner (b-SSFP, pulse repetition time/echo time = 3/1.46 ms, reconstruction matrix size: 160 × 160, 25 cardiac phases, field of view: 400 × 320 mm^2). The reference respiratory position was considered to be the end expiration at which data were acquired. The motion was assumed to be nonrigid between the reference and the other respiratory positions. To simulate data for other respiratory positions, nonrigid transformations corresponding to different radial and angular deformations were generated. To achieve this, each cardiac phase from the reference respiratory position was transformed using a nonrigid transformation Φ described by polar coordinates (r, θ) as follows:

$$\Phi : \begin{cases} r \rightarrow r f_r \left(\frac{r}{R}\right)^{\alpha} \\ \theta \rightarrow \theta + f_\theta \left(\frac{r}{R}\right)^{\beta} \end{cases} \quad [6]$$

where $0 \leq r \leq R$, R being the maximum radius in the radial direction with origin ($r = 0$) being the center of the object (heart); f_r and f_θ are the scaling parameters with f_r

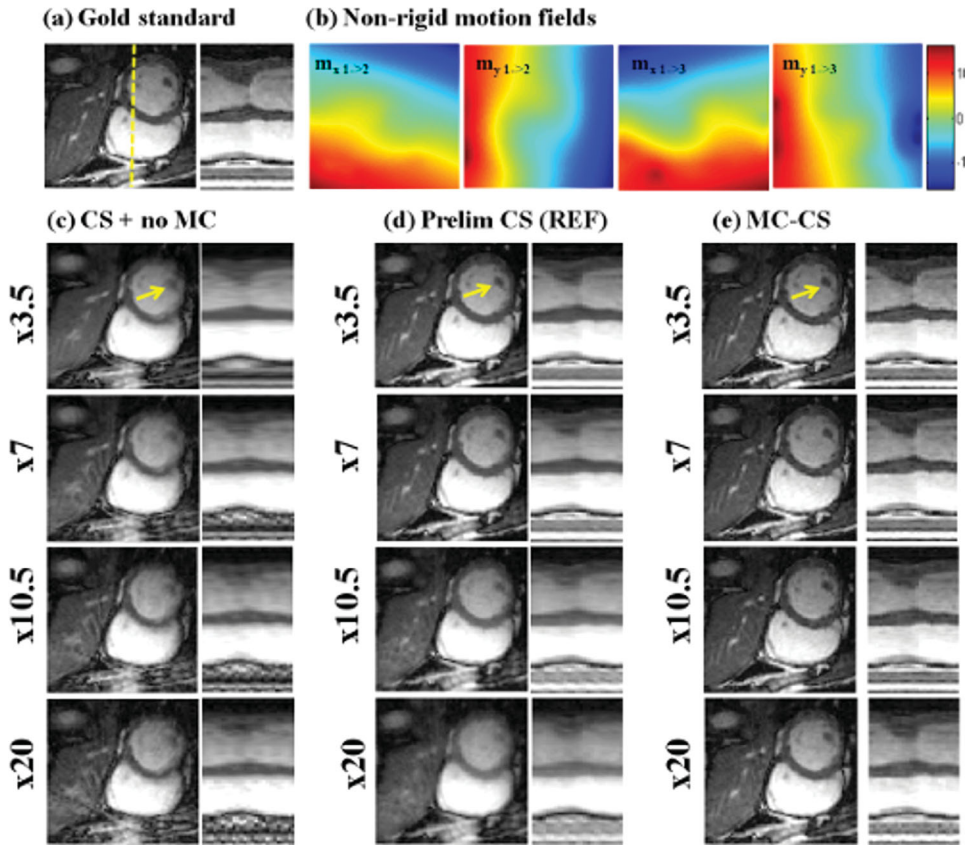

FIG. 5. Reconstruction performance of MC-CS reconstruction method on simulated motion corrupted dynamic cardiac MR data; the motion corrupted data were simulated on a golden angle radial trajectory: **(a)** From acquired fully sampled breath-held data, a gold standard fully sampled cardiac time frame and a profile corresponding to the temporal variation of pixel intensities is shown. The breath-held data were assumed to be acquired in the reference motion state (numbered 1). **b:** Two example sets of motion fields that were used to generate nonrigid transformations from reference motion state to other motion states (numbered 2 and 3) are shown. Both horizontal and vertical components of the nonrigid motion fields ($\mathbf{m}_{x\ 1\to2}$, $\mathbf{m}_{y\ 1\to2}$, $\mathbf{m}_{x\ 1\to3}$, $\mathbf{m}_{y\ 1\to3}$) are included. **c:** CS reconstruction without motion correction (CS + no MC) is shown for different acceleration factors (3.5, 7, 10.5, and 20 for each motion state), where the data from all three motion states were combined without motion correction. Strong blurring is evident in the reconstruction at all degrees of undersampling **(d)** preliminary (Prelim) standard CS reconstruction for the reference (REF) motion state. High degree of undersampling (acceleration factors of 7, 10.5, and 20) resulted in loss of high frequency components in *x–y–f* space, resulting in blurred CS reconstructions. **e:** MC-CS reconstruction using available data from all the motion states. MC-CS corrected the motion artifacts and achieved high spatial and temporal fidelity to the gold standard images in (a). [Color figure can be viewed in the online issue, which is available at wileyonlinelibrary.com.]

$\in [0,1]$ and $f_\theta \in [-\pi, \pi]$, α and β are the parameters that determine the extent of the radial and angular deformations. The parameters were chosen to yield visually plausible heart motion and were set as $f_r = 1$, $f_\theta = \pi/20$ and $\beta = 1$. Two nonrigid deformations were generated by having a different radial deformation parameter α that was set to value of 1/16 for one deformation, and $-1/16$ for the other. Including the untransformed data, the above procedure provided a sequence of cardiac phases for each of the three simulated respiratory positions. To mimic a realistic golden angle radial trajectory for sampling in k-space, a respiratory signal was obtained from a prolonged in vivo free-breathing cardiac scan comprising several heartbeats. Given the respiratory signal and the number of bins set to 3, every heartbeat in the free-breathing scan was associated with one of the three respiratory positions using the binning procedure described in the "Methods" section. The data acquisition was simulated by sampling the deformed cardiac phase sequence in each respiratory position on the golden angle radial trajectory defined by the respiratory signal. To simulate CS undersampling, the number of heartbeats from the respiratory signal was decreased such that the number of radial profiles for each cardiac phase at a specific respiratory position was reduced by acceleration factor of 3.5–20.

For each reconstruction (CS + no MC, MC-CS, and BH-CS), the overall relative root mean square (RMS) reconstruction error (Recon RMSE) for the reconstructed signal $\mathbf{x}$ (of length K) was calculated as:

$$\text{Relative RMS Error} = \sqrt{\sum_{i=1}^{K} \frac{|\mathbf{x}_i - \hat{\mathbf{x}}_i|^2}{|\mathbf{x}_i|^2}} \qquad [7]$$

where $\hat{\mathbf{x}}$ denote the reconstructed signal, and $\mathbf{x}$ is the gold standard signal reconstructed using the number of projections corresponding to the radial Nyquist rate.

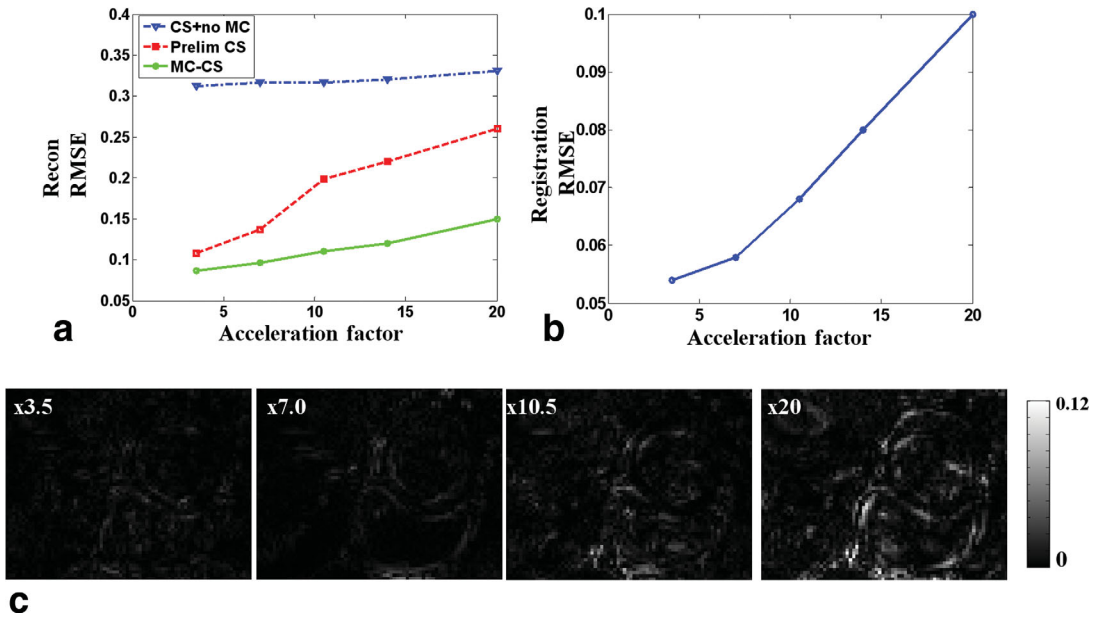

FIG. 6. **a:** Relative RMS reconstruction error (Recon RMSE) for different CS reconstructions (CS reconstruction without motion correction (CS + no MC), preliminary CS reconstruction for reference bin (Prelim CS), and proposed MC-CS reconstruction) as function of acceleration factor; **b**: relative RMS registration error (Registration RMSE) as function of acceleration factor. Both Recon RMSE and Registration RMSE were computed in a ROI containing the heart. **c:** For one of the cardiac time frames, the registration difference images (difference of image transformed with gold standard deformations and image transformed with estimated deformations) are shown as function of acceleration factor, all difference images are shown on same scale. The Registration RMSE remains low (<0.06) up to the acceleration factor of 7, as shown in the registration difference images in (c) for acceleration factors of 3.5 and 7. For higher acceleration factors, the registration error increases significantly (see registration difference images for acceleration factors of 10.5 and 20 in (c)). [Color figure can be viewed in the online issue, which is available at wileyonlinelibrary.com.]

To analyze the accuracy of the motion estimation step, for different acceleration factors, the motion fields estimated via nonrigid registrations were used to deform the untransformed images in motion state 1. The registration error (Registration RMSE) was computed using Eq. 7, where $\mathbf{x}_i$ now represents the images transformed with gold standard deformations in Eq. 6 and $\hat{\mathbf{x}}_i$ represents the images transformed with estimated deformations. Both Recon RMSE and Registration RMSE were computed in a ROI containing the heart.

To analyze the effect of selection of regularization parameter λ on the MC-CS reconstruction quality, MC-CS reconstructions were done using varying values of λ in the range of 0.0001–0.5. The Recon RMSE was computed for each case.

As there can be a number of degrees of freedom in the nonrigid motion that might occur, a number of different motion realizations were generated by varying the set of parameters f_r, f_θ, α, and β in Eq. 6. The parameters were varied randomly within 20% from their values ($f_r = 1$, $f_\theta = \pi/20$, $\beta = 1$, $\alpha = \pm 1/16$) in previous simulation such that the corresponding image transformations looked visually realistic. MC-CS reconstructions were done in each case.

In Vivo Experiments

ECG-gated free-breathing golden angle radial acquisitions were performed on Philips 1.5T in five healthy volunteers. Scan parameters include b-SSFP, pulse repetition time = 2.98 ms, echo time = 1.49 ms, field of view: 320 × 320 mm^2, spatial resolution: 1.5–2.0 mm^2, number of frequency encoding points: 160–212, 180–200 golden angle radial profiles per heartbeat, heart rate: 65–85 beats per minute (bpm), number of cardiac cycles = 25–33, scan duration = 19–25 s. Scans were performed using a 5-channel coil but a single channel (with high sensitivity over the heart) was selected for MC-CS reconstruction. The acquired free-breathing data were binned into 6–7 respiratory positions, depending on the number of heart beats, using the described adaptive binning procedure. The CS acceleration factor in each bin was set in the range of 4–6. Twenty cardiac phases were retrospectively reconstructed resulting in temporal resolution of 30–40 ms. For comparison, the breath-held data were acquired at the end-expiration state in all the volunteers with the same imaging parameters, except that the scan duration was reduced (number of cardiac cycles = 13–29, acquisition time = 10–20 s).

RESULTS

Simulations

The gold standard fully sampled reconstruction for one of the cardiac time frames is shown in Figure 5a. A gold standard fully sampled temporal profile corresponding to the temporal variation of pixel intensities along the dotted line is also shown. Two example sets of motion fields corresponding to the nonrigid transformations from breath-hold reference motion state 1 to motion

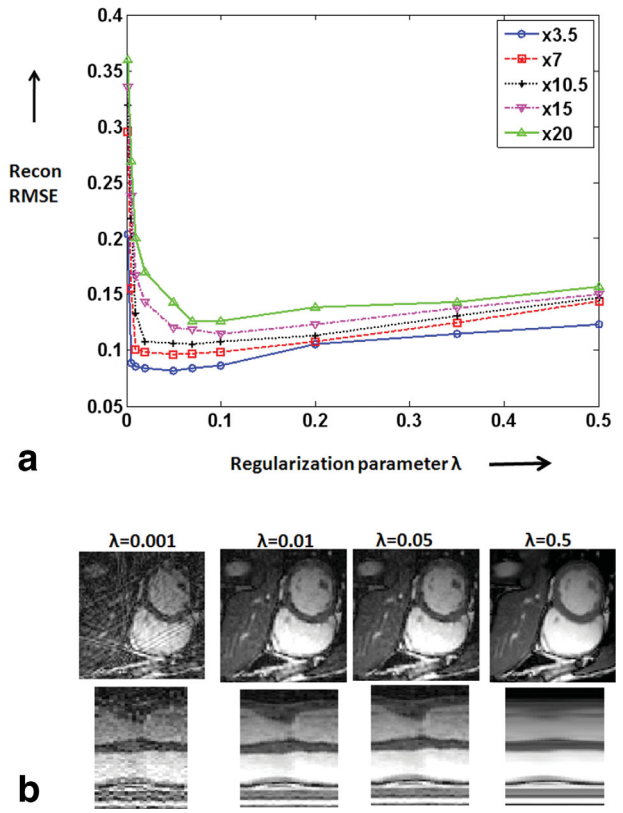

FIG. 7. **a:** MC-CS relative RMS reconstruction error (Recon RMSE) as a function of regularization parameter (λ) in Eq. 4 for different acceleration factors (×*R*). The parameter λ in the range 0.01–0.1 gave comparable reconstruction results and low values of RMSE **(b)** MC-CS reconstructions for different values of λ with 7-fold acceleration; an example reconstructed cardiac frame and temporal profile are shown. Too low values (λ = 0.001) resulted in appearance of undersampling artifacts in the reconstruction; too high values (λ = 0.5) resulted in blurry reconstruction. [Color figure can be viewed in the online issue, which is available at wileyonlinelibrary.com.]

states 2 and 3 are shown in Figure 5b. Both horizontal and vertical components of the motion fields ($\mathbf{m}_{x\ 1\to2}$, $\mathbf{m}_{y\ 1\to2}$, $\mathbf{m}_{x\ 1\to3}$, $\mathbf{m}_{y\ 1\to3}$) are shown. Relative to the Nyquist sampling rate ($160 \times \pi/2 \sim 251$ profiles) required for each cardiac phase, acceleration factors of 3.5, 7, 10.5, 15, and 20 were simulated for k-space data in each of the three respiratory positions. The CS reconstructed cardiac frames and temporal profiles are shown in Figure 5c–e. Strong blurring artifacts due to nonrigid motion were evident in the CS reconstruction without motion correction (CS + no MC) for all acceleration factors (Fig. 5c). The preliminary CS reconstruction for the reference breath-hold position is shown in Figure 5d. The preliminary CS reconstructions at other respiratory positions (not shown here) were of similar or lower quality. At an acceleration factor of 3.5 (72 golden angle radial profiles per cardiac phase), all preliminary CS reconstructions had good quality, and the expected variations in the temporal profile were observed. However, at higher acceleration factors of 7, 10.5, and 20, the preliminary CS reconstructions tend to become blurrier. MC-CS reconstruction (Fig. 5e) visually corrected for blurriness in the combined motion corrected images and had high spatial and temporal fidelity to the gold standard images in Figure 5a.

A plot of relative RMS reconstruction error (Recon RMSE) in the ROI containing the heart for different CS reconstructions as a function of acceleration factor is shown in Figure 6a. Although not reported in the manuscript, the reconstruction error was stronger in the region outside the ROI than inside, as both registration and CS reconstruction favor high contrast components for alignment and reconstruction, and region outside the ROI contains mainly the low contrast components.

The RMS registration error (Registration RMSE) as a function of acceleration factor is shown in Figure 6b. For different acceleration factors, the registration error difference images (difference of an image transformed with gold standard deformation and image transformed with estimated deformation) for one of the cardiac time frames are also shown in Figure 6c. The registration error remains low (Registration RMSE < 0.06) up to the acceleration factor of 7. For higher acceleration factors, the registration error increases significantly (see registration difference images for acceleration factors of 10.5 and 20 in Fig. 6c).

A plot of Recon RMSE as a function of regularization parameter λ is shown in Figure 7a for different acceleration factors. The RMSE remained low and MC-CS reconstructions looked comparable (not shown here) in the range of $\lambda = 0.01$–0.1. MC-CS reconstructions for different values of λ with 7-fold acceleration are shown in Figure 7b. For $\lambda > 0.1$, the MC-CS reconstructions tend to become blurry, losing some of the variations in the temporal profiles. For $\lambda < 0.01$, the MC-CS reconstructions tend to become noisy with undersampling artifacts.

For 20 different nonrigid motion realizations achieved with different values of set of parameters (f_r, f_θ, α, and β) in Eq. 6, MC-CS method corrected for nonrigid motion in each case and gave similar reconstruction quality and

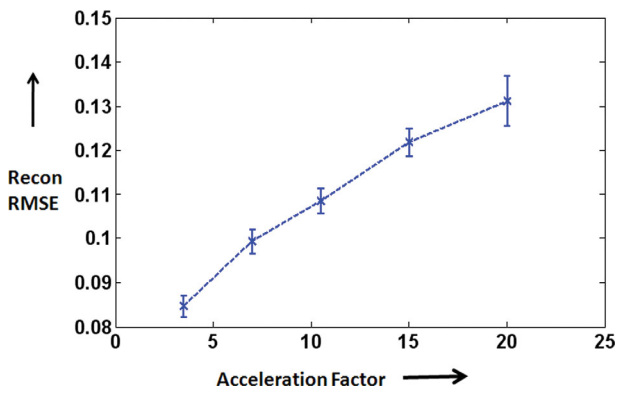

FIG. 8. For 20 different nonrigid motion realizations simulated by variation of motion parameters in Eq. 6, plot of mean value of MC-CS relative RMS reconstruction error (Recon RMSE) is shown as a function of acceleration factor, the standard deviation of RMSE is also indicated at each acceleration factor. [Color figure can be viewed in the online issue, which is available at wileyonlinelibrary.com.]

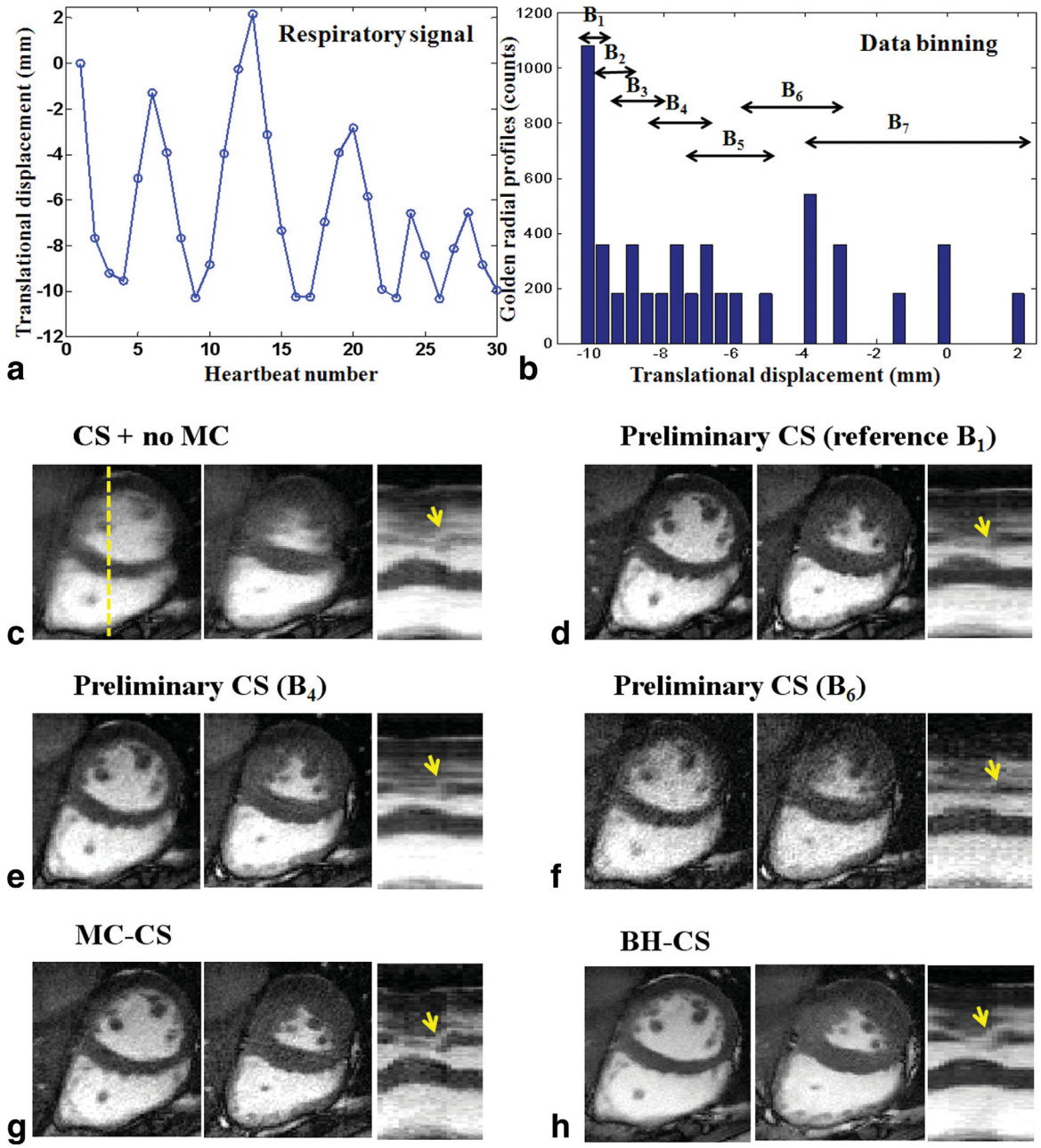

FIG. 9. Results of different steps of proposed method for in vivo data from volunteer 1: a free-breathing scan of 30 heart beats was performed on a healthy volunteer, each *R–R* interval comprised 180 golden angle radial profiles. A respiratory signal (shown in **(a)**) was obtained from registration of virtual navigator (vNAV) images reconstructed from golden angle radial profiles acquired in each heart beat. This respiratory signal was then used for retrospectively binning of cardiac data into different respiratory motion states/bins. Distribution of number of golden angle radial profiles at different displacement values of respiratory signal are shown in **(b)**. Different bins (B_1–B_7) formed are shown, the data in each bin corresponded to approximate acceleration factor of 5.3 relative to the Nyquist rate. **c:** Results of CS reconstruction without motion correction (CS + no MC), both diastole and systolic cardiac phases are shown together with a temporal profile corresponding to the temporal variation of pixel intensities along the dotted line (**d-f**) preliminary standard CS reconstructions for reference (REF) bin B_1 and two other bins (B_4 and B_6) at different respiratory positions are shown. **g:** Proposed MC-CS reconstruction using data available from all bins. The MC-CS reconstructed images had higher spatial and temporal quality compared to CS + no MC and all preliminary CS reconstructions (arrows in (c)-(g)). **h:** CS reconstruction from data acquired in a breath-held scan (BH-CS), the breath-hold scan comprised 29 heart beats acquired at end-expiration state.

values of RMSE. A plot of mean Recon RMSE obtained from MC-CS results with 20 different nonrigid motion realizations is shown in Figure 8. The standard deviation of reconstruction error is also indicated for each acceleration factor.

In Vivo Experiments

For volunteer 1, the respiratory signal obtained from the vNAV images is shown in Figure 9a (from a 20 s free-breathing scan comprising 30 heart beats).The result of

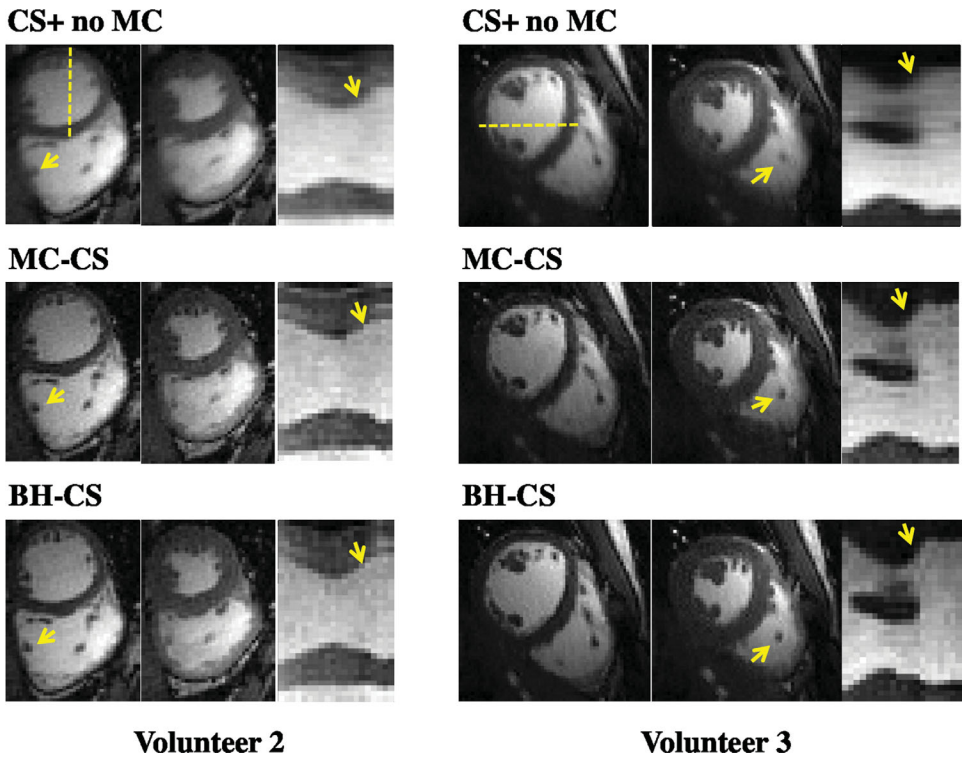

FIG. 10. Performance comparison of different CS reconstructions for in vivo data from volunteers 2 and 3; the free-breathing scans for volunteers 2 and 3 comprised 25 and 33 heart beats, respectively. Data were binned into six and seven respiratory positions for volunteers 2 and 3, respectively. CS reconstructed frames during both systole and diastole are shown together with the temporal variation of pixel intensities along the dotted lines. CS reconstruction without motion correction (CS + no MC), proposed MC-CS reconstruction and CS reconstruction from breath-hold acquisition (BH-CS) are shown. The breath-hold scans were of 10- and 15-s duration, and comprised 13 and 20 heart beats for volunteers 2 and 3, respectively. Proposed MC-CS reconstruction corrected for most of the blurring in CS + no MC reconstruction and had similar spatial and temporal quality than the BH-CS reconstruction (see the region pointed by arrows). [Color figure can be viewed in the online issue, which is available at wileyonlinelibrary.com.]

the proposed data binning strategy is shown in Figure 9b, which shows the distribution of the number of golden angle radial profiles at different displacement values of the vNAV images. The preliminary CS reconstructions for the reference bin (B_1), and bins at two other respiratory positions (B_4 and B_6) are shown in Figure 9d–f. The data in the reference bin and other bins correspond to an acceleration factor of 5.3. The MC-CS reconstruction (Fig. 9g) corrected for most of the artifacts in CS + no MC (Fig. 9c) reconstruction. The MC-CS reconstructed images were better in quality than all preliminary CS reconstructions (Fig. 9d–f) and were visually of similar quality as the BH-CS reconstruction (Fig. 9h) from breath-hold acquisition of approximately the same duration (19.5 s).

The MC-CS reconstructed cardiac frames and temporal profiles for two other volunteers (volunteers 2 and 3) are shown in Figure 10, in comparison with the noncorrected (CS + no MC) and reconstruction from breath-held (BH-CS) acquisitions. Figure 10 shows that MC-CS reconstruction achieved similar quality to the breath-hold images.

DISCUSSION

This work proposes a CS motion corrected reconstruction from undersampled general (affine or nonrigid) motion corrupted dynamic cardiac MR data. The proposed method is a combination of CS (4) and the motion correction technique by Batchelor et al. (12) and can correct for arbitrary motion in the CS reconstruction. The use of the proposed method is demonstrated in 2D gated cardiac CINE MRI, where 20 respiratory-motion free cardiac phases were reconstructed with high spatial and temporal fidelity to the breath-held images, resulting in a temporal resolution of 30–40 ms. The flexibility of the golden angle radial acquisition was used for respiratory self-gating and adaptive binning in free-breathing dynamic cardiac MRI. The proposed approach permits free-breathing acquisitions, and further studies may explore its application to 3D dynamic cardiac MRI.

While motion correction methods have been well integrated into parallel imaging (14,15,21,22), CS-based reconstruction methods integrated with motion correction have been only shown for rigid motion. Compared to parallel imaging methods that reconstruct each cardiac phase/frame independently, the proposed MC-CS framework for dynamic cardiac MRI exploits redundancy along the temporal dimension by finding the sparsest solution in the spatio-temporal x–y–f space.

At high acceleration factors (undersampling factor of 7 in each cardiac phase in Fig. 5d), due to insufficient number of measurements in each bin, the preliminary CS reconstructions are unable to reconstruct high frequency temporal components in the x–y–f space and

lead to slightly blurred reconstructions. However, these slightly blurred reconstructions are still good enough to estimate precise nonrigid motion between different motion states (RMS registration error < 0.06 for 7-fold acceleration, Fig. 6b,c). Using the estimated motion fields, the MC-CS is able to correct the nonrigid motion in the final reconstruction with high spatial and temporal fidelity compared to the gold standard reconstruction in Figure 5a. At very high acceleration factors (acceleration factor of 20 per cardiac phase Fig. 5d), the preliminary CS reconstructions suffer from strong undersampling artifacts, and the image quality is not good enough to get precise motion between different respiratory positions (Registration RMSE ~ 0.10, see registration difference images in Fig. 6c), hence the final MC-CS reconstruction still suffers from some blurring artifacts.

We used an adaptive binning procedure for data acquired in 19–25 s free-breathing scans, comprising 25–33 cardiac cycles. The number of bins was in the range of 6–7 depending on the number of acquired heartbeats. The size of each bin was adjusted to guarantee undersampling factors of 4–6 for each bin for preliminary CS reconstruction. This resulted in preliminary CS reconstructions of sufficient quality to achieve accurate registrations and good quality subsequent MC-CS reconstructions. The number of bins was set to be higher than five overlapping windows to get an average bin width of 2 mm. If too few bins are used (<3), this will lead to strong intrabin motion and motion artifacts remaining in the reconstruction despite having more than sufficient amount of data in each bin for the CS reconstruction. If too many bins are used, preliminary CS reconstructed images may not have enough quality to ensure accurate nonrigid motion estimation. In the experiments, we have used data available from all bins in the final MC-CS reconstruction. To further improve the reconstruction, the data corresponding to bins having larger widths (greater than 4 mm, for example) could be rejected for MC-CS reconstruction to avoid high intrabin motion.

The proposed approach corrects for respiratory motion during free-breathing cardiac acquisition, but correction for heart-rate variability is not considered in this work. Hence, further modifications will be needed to apply the proposed method in arrhythmic patients. In our work, we have assumed that all cardiac phases are in the same respiratory motion state. However, the golden radial trajectory offers the option of reconstructing multiple navigator images (vNAV) for different cardiac phases, which will be investigated in future work.

The MC-CS framework is computationally more complex compared to the standard CS reconstruction, as preliminary CS reconstructions have to be performed for each bin and additionally for the final MC-CS step. With a nonoptimized MATLAB based implementation, the average time for reconstruction of motion corrected images from in vivo free-breathing data was in the range of 2–2.5 h, whereas for breath-held data it was in the range of 15–30 min. However, several steps of the proposed framework are highly parallelizable and the reconstruction time might be reduced using parallel computing techniques.

The proposed method has preliminary CS reconstruction, motion estimation, and final MC-CS reconstruction as sequential stages. One of the limitations of such architecture is that errors in any stage are propagated to the next one. A possible way around this would be to combine all steps into one coupled problem, using an approach similar to generalized reconstruction by inversion of coupled systems (GRICS) (14), where the image reconstruction and the motion estimation steps are combined into one coupled optimization problem, leading to an autocalibrated motion model.

In the motion estimation step of the proposed method, we have used intensity-based nonrigid registration algorithm (25) to estimate nonrigid motion between different respiratory positions. Instead of using registrations, block based dense motion field estimation as done in k-t FOCUSS (9–11) might be used for motion estimation.

The use of MC-CS framework may be extended to alternative applications where the respiratory signal can be used as a motion surrogate signal. An example of this is motion corrected liver MRI. In other applications where a motion surrogate signal is not available for data binning, further novel motion correction techniques need to be developed.

CONCLUSIONS

A novel reconstruction framework was presented for dynamic cardiac MRI that benefits from the high acceleration available with CS and correction for arbitrary (affine or nonrigid) motion in the CS reconstruction. The use of this framework was demonstrated in 2D cardiac gated MRI using a golden radial acquisition, where respiratory motion-free cardiac phases were reconstructed from undersampled self-gated free-breathing k-space data.

ACKNOWLEDGMENTS

The authors dedicate this article to the loving memory of our wonderful colleague, Philip G. Batchelor. C. Prieto acknowledges financial support from FONDECYT. The authors thank Michael Lustig for making the nonlinear conjugate gradient MATLAB code available online.

REFERENCES

1. Donoho DL. Compressed sensing. IEEE Trans Inform Theory 2006;52:1289–1306.
2. Candes E. Compressive Sampling. In: Proceedings of International Congress of Mathematicians, Vol. 3, Madrid, Spain, 2006. pp 1433–1452.
3. Lustig M, Donoho D, Pauly JM. Sparse MRI: the application of compressed sensing for rapid MR imaging. Magn Res Med 2007;58:1182–1195.
4. Lustig M, Santos JM, Donoho DL, Pauly JM. k–t SPARSE: High Frame Rate Dynamic MRI Exploiting Spatio-Temporal Sparsity. In Proceedings of the 13th Annual Meeting of ISMRM, Seatle, Washington, USA, 2006. p. 2420.
5. Akcakaya M, Nam S, Hu P, Moghari MH, Ngo LH, Tarokh V, Manning WJ, Nezafat R. Compressed sensing with wavelet domain dependencies for coronary MRI: a retrospective study. IEEE Trans Med Imaging 2011;30:1090–1099.
6. Vasanawala SS, Alley MT, Hargreaves BA, Barth RA, Pauly JM, Lustig M. Improved pediatric MR imaging with compressed sensing. Radiology 2010;256:607–616.
7. Otazo R, Kim D, Axel L, Sodickson DK. Combination of Compressed Sensing and Parallel Imaging with Respiratory Motion Correction for

Highly-Accelerated First-Pass Cardiac Perfusion MRI. In Proceedings of the 18th Annual Meeting of ISMRM, Montreal, Canada, 2011. p. 63.
8. Doneva M, Stehning C, Nehrke K, Börnert P. Improving Scan Efficiency of Respiratory Gated Imaging Using Compressed Sensing with 3D Cartesian Golden Angle Sampling. In Proceedings of the 19th Annual Meeting of ISMRM, Montreal, Canada, 2011. p. 624.
9. Jung H, Sung K, Nayak KS, Kim EY, Ye JC. k-t FOCUSS: a general compressed sensing framework for high resolution dynamic MRI. Magn Res Med 2009;61:103–116.
10. Jung H, Park J, Yoo J, Ye JC. Radial k-t FOCUSS for highresolution cardiac cine MRI. Magn Res Med 2010;63:68–78.
11. Jung H, Ye JC. Motion estimated and compensated compressed sensing dynamic magnetic resonance imaging: what we can learn from video compression techniques. Int J Imaging Syst Technol 2010;20: 81–98.
12. Batchelor PG, Atkinson D, Irarrazaval P, Hill DLG, Hajnal J, Larkman D. Matrix description of general motion correction applied to multishot images. Magn Res Med 2005;54:1273–1280.
13. Schmidt JFM, Buehrer M, Boesiger P, Kozerke S. Nonrigid retrospective respiratory motion correction in whole-heart coronary MRA. Magn Res Med 2011;66:1541–1549.
14. Odille F, Vuissoz PA, Marie PY, Felblinger J. Generalized reconstruction by inversion of coupled systems (GRICS) applied to free-breathing MRI. Magn Res Med 2008;60:146–157.
15. Hansen M, Sorensen T, Arai A, Kellman P. Retrospective reconstruction of high temporal resolution cine images from real-time MRI using iterative motion correction. Magn Reson Med 2011. doi: 10.1002/mrm.23284.
16. Odille F, Cindea N, Mandry D, Pasquier C, Vuissoz PA, Felblinger J. Generalized MRI reconstruction including elastic physiological motion and coil, sensitivity encoding. Magn Res Med 2008;59: 1401–1411.
17. White MJ, Hawkes DJ, Melbourne A, Collins DJ, Coolens C, Hawkins M, Leach MO, Atkinson D. Motion artifact correction in free-breathing abdominal MRI using overlapping partial samples to recover image deformations. Magn Res Med 2009;62:440–449.
18. Winkelmann S, Schaeffter T, Koehler T, Eggers H, Doessel O. An optimal radial profile order based on the golden ratio for time-resolved MRI. IEEE Trans Med Imaging 2007;26:68–76.
19. Chan RW, Ramsay EA, Cheung EY, Plewes DB. The influence of radial undersampling schemes on compressed sensing reconstruction in breast MRI. Magn Res Med 2012;67:363–377.
20. Jung H, Park J, Yoo J, Ye JC. Radial k-t FOCUSS for high-resolution cardiac cine MRI. Magn Res Med 2010;63:68–78.
21. Kellman P, Chefd'hotel C, Lorenz CH, Mancini C, Arai AE, McVeigh ER. High spatial and temporal resolution cardiac cine MRI from retrospective reconstruction of data acquired in real time using motion correction and resorting. Magn Res Med 2009;62: 1557–1564.
22. Kellman P, Chefd'hotel C, Lorenz CH, Mancini C, Arai AE, McVeigh ER. Fully automatic, retrospective enhancement of real-time acquired cardiac cine MR images using image-based navigators and respiratory motion-corrected averaging. Magn Res Med 2008;59:771–778.
23. Jhooti P, Gatehouse PD, Keegan J, Bunce NH, Taylor AM, Firmin DN. Phase ordering with automatic window selection (PAWS): a novel motion-resistant technique for 3D coronary imaging. Magn Res Med 2000;43:470–480.
24. Buerger C, King AP, Schaeffter T, Prieto C. 3D non-rigid motion modelling of the liver from undersampled Golden-Radial Phase encoding (G-RPE) acquisitions. In Proceedings of the 18th Annual Meeting of ISMRM, Montreal, Canada, 2011. p. 643.
25. Buerger C, Schaeffter T, King AP. Hierarchical adaptive local affine registration for fast and robust respiratory motion estimation. Med Image Anal 2011;15:551–564.
26. Jackson JI, Meyer CH, Nishimura DG, Macovski A. Selection of a convolution function for fourier inversion using gridding. IEEE Trans Med Imaging 1991;10:473–478.
27. Rasche V, Proksa R, Sinkus R, Bornert P, Eggers H. Resampling of data between arbitrary grids using convolution interpolation. IEEE Trans Med Imaging 1999;18:385–392.